Theor Chem Acc (2011) 130:829–837
DOI 10.1007/s00214-011-1055-0

REGULAR ARTICLE

Interaction of Fe^{3+}meso-tetrakis (2,6-dichloro-3-sulfonatophenyl) porphyrin with cationic bilayers: magnetic switching of the porphyrin and magnetic induction at the interface

Katia C. U. Mugnol · Marccus V. A. Martins · Edvaldo C. Nascimento · Otaciro R. Nascimento · Frank N. Crespilho · Jeverson T. Arantes · Iseli L. Nantes

Received: 30 May 2011 / Accepted: 19 September 2011 / Published online: 29 October 2011

Abstract An organized multilayer was constructed by the layer-by-layer technique in which alternating layers of metalloporphyrin and dioctadecyldimethylammonium bromide bilayers were deposited onto an indium tin oxide surface electrode. The porphyrin molecules that are organized in the different layers showed a strong electroactivity with a well-defined electrochemical process. In LbL, electroactivity could be explained only by the occurrence of electron hoping. Thus, total Kohn–Sham density functional theory (KS-DFT) was performed to better understand the conditions responsible for the electroactivity of the metalloporphyrin layers intercalated by an insulating material. Total KS-DFT theory involves local density approximation energy calculations based on spin-polarized variant of KS-DFT theory. The results revealed a magnetization switching of the metalloporphyrin induced by the interaction with the surfactant bilayer accompanied by spin polarization of the porphyrin-interacting surfactant molecule. Although discrete, the surfactant magnetization had significant repercussions on the electron conductivity. Calculations also demonstrated loss of porphyrin symmetry promoted by a parent surfactant with a shorter hydrocarbon chain, ditetradecyldimethylammonium bromide. The calculation results were corroborated by experimental results obtained by the electron paramagnetic resonance and magnetic circular dichroism techniques.

Keywords KS-DFT · Spin polarization · Fe^{3+}Meso-tetrakis (2,6-dichloro-3-sulfonatophenyl) Porphyrin · Lipid bilayer · Magnetizability · Electron conductivity

1 Introduction

Metalloporphyrins are very versatile molecules that were selected by nature to act in a variety of biological functions, such as electron transfer, light harvesting antennas, biocatalysis, molecular oxygen transport, cell signaling, and even cell death [1–11].

Biological and synthetic porphyrins are of increased interest due to their use in the design and build-up of supramolecular structures, some of which have been applied successfully in various nanotechnological applications [12–14]. One particular interest is the use of porphyrins for spin-dependent electron transport through biomolecular devices. The quasiplanar geometries of metalloporphyrins have given these molecules the potential to form stacked layers, the properties of which can be used to form two-dimensional assemblies and used in electronic circuits or devices [15–18]. On the other hand, the normally six-coordinate metal center with its four porphyrin ring nitrogen atoms allows the addition of two axial

Dedicated to Professor Akira Imamura on the occasion of his 77th birthday and published as part of the Imamura Festschrift Issue.

K. C. U. Mugnol · M. V. A. Martins · E. C. Nascimento · O. R. Nascimento · F. N. Crespilho · I. L. Nantes (✉)
Centro de Ciências Naturais e Humanas (CCNH), Universidade Federal do ABC, Rua Santa Adélia, 166, Santo André, SP 09210-170, Brazil
e-mail: ilnantes@ufabc.edu.br

O. R. Nascimento
Grupo de Biofísica "Sergio Mascarenhas", Universidade de São Paulo, São Carlos, SP, Brazil

J. T. Arantes (✉)
Centro de Engenharia, Modelagem e Ciências Sociais Aplicadas (CECS), Universidade Federal do ABC, Rua Santa Adélia, 166, Santo André, SP 09210-0170, Brazil
e-mail: jeverson.teodoro@ufabc.edu.br

ligands. For design purposes, these axial ligand sites are important for the control of porphyrin properties [19, 20].

By mimicking biological porphyrin systems, the properties of the designed synthetic porphyrins have been able to be modulated by changing the microenvironment in various arrangements, such as association with polymers, and embedded in micelles and liposomes [21]. The structures of these molecular complex constructs are maintained by the weaker (than in many cases non-reversible covalent bonding) and reversible non-covalent interactions, such as metal–ligand coordinate bonding, hydrogen-bonding, aromatic π–π stacking, and hydrophobic interactions. The study of this group of molecules, molecular complexes and aggregates, and the forces and interactions within them, and between these molecules, and finally their interactions with the solvent and more complex environments constitutes a branch of chemistry commonly referred to as supramolecular chemistry [22–28].

The molecular interactions responsible for the stability of supramolecular structures are weak forces and consequently they require calculations with a high level of chemical accuracy [29–33]. Considering that single reference Hartree–Fock wave function theory (WFT) quantum mechanics and local density approximation (LDA) and even the generalized gradient approximation (GGA) KS-DFT do not have the accuracy required for the calculation of weak van der Waals-dispersion interactions/forces, both WFT and KS-DFT needed to be extended and even reformulated to be applied for the dispersion forces and interactions that are responsible for the stability of the noble gas dimers and stacked aromatics compounds. Within KS-DFT theory, the so-called dispersion correction has been used [34], while in WFT, the methods commonly used are WFT electron correlation, that are known as correlated methods such as complete active space perturbation theory (CASPT2) [35] or multi-reference couple cluster (MR-CC) methods [36–40]. These are two of the most accurate WFT methods which are able to quantitatively treat the types of interactions and forces responsible for the stability of the structures in supramolecular chemistry, physics, and materials science. Complementary experimental and theoretical studies concerning supramolecular structures are relevant due to the wide application of these systems in the nanotechnological area. Supramolecular chemistry allows for tremendous possibilities to produce different molecular architectures such as the ultra-fine films, especially hybrid nanoarchitectures, which are held together by non-covalent forces and interactions [41–43]. By using strategies such as the promising layer-by-layer deposition technique (LbL films), different compounds can be assembled into nanodevices [44–46]. An equally promising strategy related to the use of porphyrins is the induced magnetization of these molecules (spin polarization). Molecular spintronic materials constructed/assembled with organic molecules are promising for the design of interfaces with tunable magnetic and electronic interactions and depend very much on the structure of the organic or bioorganic compounds. In addition, the organic-containing spintronic devices present potentially lower processing costs compared to inorganic materials due to the use of changing and optimizing solvents, pH, ionic strength and other variables that are much easier and common to manipulate that those required in inorganic chemistry. A common strategy to induce magnetic order and switching in metalloporphyrin systems is the deposition of the molecules onto a ferromagnetic metal surface leading to the parallel alignment of spin of the central ion with the substrate magnetization [10–12]. However, other types of interactions that are able to promote magnetization switching in porphyrin systems remain to be investigated. To the best of our knowledge, we report here for the first time the magnetization switching in a porphyrin system induced by the interaction of the porphyrin molecules, i.e., Fe^{3+}meso-tetrakis (2,6-dichloro-3-sulfonatophenyl) porphyrin (Fig. 1), in the deposited layer with a surfactant bilayer accompanied by spin polarization of the surfactant molecules in the adjacent monolayers. Although discrete, the surfactant magnetization has significant effects on the electron conductivity, which will need to be taken into account in any nanotechnological applications that may use this technology.

2 Materials and methods

2.1 Chemicals

Reagents used included meso-tetrakis (2,6-dichloro-3-sulfonatophenyl) porphyrin ($Fe^{3+}TDCSO_3^-Na^+PP$), dioctadecyldimethylammonium bromide (DODAB), and sodium

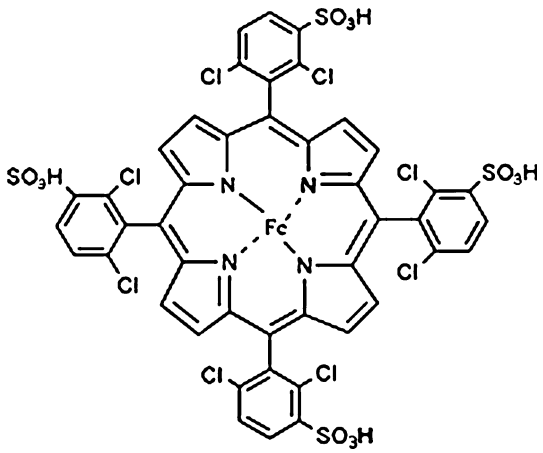

Fig. 1 Structure of Fe^{3+}Meso-tetrakis (2,6-dichloro-3-sulfonatophenyl) Porphyrin

phosphate obtained from Sigma Chemical (St. Louis, MO) and tris–HCl (Aldrich, Milwaukee, WI). All reagents were of analytical grade and used without further purification.

2.2 Giants unilamelar vesicles preparation

Dioctadecyldimethylammonium bromide (DODAB) was obtained from Sigma Chemical Co. and used as such without further purification. Stock solutions of DODAB giant vesicles were prepared by mixing DODAB and distilled and deionized water to a desired final concentration (500 μM) and then warmed at 60 °C for 20 min, followed by 5 min cooling with vortex agitation. These warming and cooling cycles were repeated three times [22]. To be able to manipulate/control/vary the porphyrin systems, after the DODAB vesicle preparation, we added 20 μM $Fe^{3+}TDCSO_3^-Na^+PP$ prepared in 5 mM pH 7.4 sodium phosphate buffer solution.

2.3 CD and MCD measurements

The circular dichroism (CD) and magnetic circular dichroism (MCD) measurements were carried out using a Jasco J-720 spectropolarimeter (Easton, MD) using quartz cuvettes with a 0.1-cm optical path; *a* band width, 1.0 nm; a scanning speed, 100 nm/min; a response, 1 s; and 2 accumulations. For the MCD measurements, the magnetic field was 870 mT. The magnet was from Jasco and designed for the use for MCD spectral measurements.

2.4 Manufacture of LBL films ITO-(DODAB/$Fe^{3+}TDCSO_3^-Na^+PP$)

Before being used to manufacture electrodes, the ITO substrates (glass coated with indium tin oxide) were cleaned by heating them in acetone for 10 min followed by rinsing with distilled water (Milli-Q system) and heating at 60 °C for 10 min in a 6:1:1 solution of distilled water : 30% H_2O_2 : concentrated NH_4OH. Then, the ITO substrates were again washed with distilled water. ITO-(DODAB/$Fe^{3+}TDCSO_3^-Na^+PP$) electrodes were produced by the layer-by-layer (LbL) technique proposed by Decher [46, 47]. Briefly, the sequential layer arrangement of DODAB and $Fe^{3+}TDCSO_3^-Na^+PP$ on the negatively charged substrate (ITO) of LbL films was governed by electrostatic interactions between species bearing opposite charges [24] that are sequentially deposited onto the substrate by alternating immersion of the substrate in DODAB and $Fe^{3+}TDCSO_3^-Na^+PP$ solutions interspersed by washing in distilled water (Fig. 2). A schematic diagram illustrating the LbL technique is also shown in Fig 2. As shown in this figure, the negatively charged substrate (ITO) was immersed in a solution of 1 mM DODAB for 5 min leading to the adsorption of the first positively charged layer. Subsequently, the substrate containing the monolayer was washed in distilled water (Milli-Q) and dried with nitrogen gas. In sequence, the modified substrate was immersed for 5 min in a solution of 1 mM $Fe^{3+}TDCSO_3^-Na^+PP$ leading to the adsorption of the negatively charged layer. Subsequently, the substrate containing a bilayer was washed in another washing solution (PBS, pH 7.0) and dried with nitrogen gas. This procedure was repeated five times to obtain a film with 5 bilayers.

2.5 Electrochemical measurements

Voltammetry experiments were carried out using a potentiostat/galvanostat μAutolab with the GPES software. We used a conventional system of three electrodes: indium tin oxide (ITO) coated glass (and ITO-DODAB/$Fe^{3+}TDCSO_3^-Na^+PP$) as the working electrode, a platinum sheet as the auxiliary electrode, and $Ag/AgCl_{sat}$ as the reference. The supporting electrolyte was a phosphate buffer solution (1 mol L^{-1}). All experiments were conducted in thoroughly nitrogen deaerated solutions at a temperature of 24 °C.

2.6 KS-DFT calculations

The theoretical results were obtained via total energy KS-DFT calculations based on the spin-polarized variant of KS-DFT, within the LDA, and employing the projected augmented wave method (PAW) [48]. A plane wave basis set expansion up to 464.51 eV, as implemented in the VASP code, was used [49]. All atoms were allowed to relax until the forces in each Cartesian coordinate became smaller than 0.025 eV/Å. First we calculated the isolated systems (porphyrin and ditetradecyldimethylammonium bromide (DTDAB)). DTDAB was used rather than DODAB in our work here. A unit cell with cell dimensions of 20 × 60 × 15 ångstroms in *x*, *y*, and *z* directions, respectively, was used to prevent spurious interactions between the image and the unit cell in our periodic boundary condition calculations. Subsequently, we calculated the properties of the DTDAB-porphyrin system. It is known that in many cases, it is necessary to go beyond the LDA KS-DFT level [50] to get a better description of molecular solids, but in our theoretical study here, we are initially investigating the interactions in the isolated systems and then the combined system. The porphyrin was placed together in the unit cell with the DTDAB at a distance in accordance with the π–π stacking geometry and subsequently we permitted the whole system to relax (full geometry optimization). Although the dispersion/van der Waals type interactions may not be well described at the LDA KS-DFT level, we believe (hypothesize) that the total energy differences will be very small when compared with those calculated using the more sophisticated KS LC-DFT, KS-LC_{gau}-DFT, KS LC-DFT+LRD, and KS-

LC_{gau}-DFT+LRD methods [34] and even though our conclusions may change quantitatively, they will not change qualitatively. The local net magnetization was also investigated and for this property, we used the spin density defined by $m(\vec{r}) = \rho_{up}(\vec{r}) - \rho_{down}(\vec{r})$.

3 Results and discussion

Considering the potential interaction of the oppositely charged $Fe^{3+}TDCSO_3{}^{-}Na^{+}PP$ and the surfactant DODAB with respect to the effects on the porphyrin properties, an organized multilayer was constructed by the layer-by-layer (LbL) technique. The number of bilayers was chosen based on previous results, in which it was reported that the thickness of LbL films affects the charge transport mechanism within the multilayers. [42, 51–54]. This mechanism was first introduced by Laurent and Schlenoff [55] where it was reported that the transport of charges within alternating layers of polyelectrolytes is due to a maximum distance of a few ångstroms between layers that allows for tunneling of the electrons. In alternating layers of metalloporphyrin and surfactants, electroactivity could be expected only by the occurrence of electron hoping [47–49]. Figure 3 shows the redox processes of the system deposited onto the ITO electrode that was analyzed by cyclic voltammetry experiments. As the cationic DODAB does not exhibit redox processes (data not shown), all processes are assigned to $Fe^{3+}TDCSO_3{}^{-}Na^{+}PP$. The porphyrin molecules organized into different layers presented strong electron activity with a well-defined electrochemical process (SI) associated to the redox processes of metalloporphyrin (Fig. 3).

The voltammogram presented in Fig. 3 shows two anodic and cathodic peaks. The most probable occurrences for the observed results are redox processes of the central iron ion (Epa^1, Epc^2) and the porphyrin ring (Epa^2, Epc^1). However, other alternative processes should be also considered and discussed. The occurrence of two metal-centered redox processes is improbable because the electrochemistry analysis started with $(TDCSO_3PP)^{4-}]Fe^{3+}$ oxidation, and porphyrin Fe^{5+} has not been described in the literature. Another possibility to be considered is the assignment of the pair of anodic and cathodic peaks to two populations of porphyrin exhibiting different conformations. By assuming the different redox potentials as linked to the porphyrin conformations, the values obtained here might be assigned exclusively to ring-centered processes of two porphyrin populations. In fact, as depicted below, EPR and magnetic circular dichroism (MCD) of $(TDCSO_3PP)^{4-}]Fe^{3+}$ associated to DODAB bilayers were consistent with the presence of two porphyrin conformations induced by the association with the surfactant. However, literature data have reported the occurrence

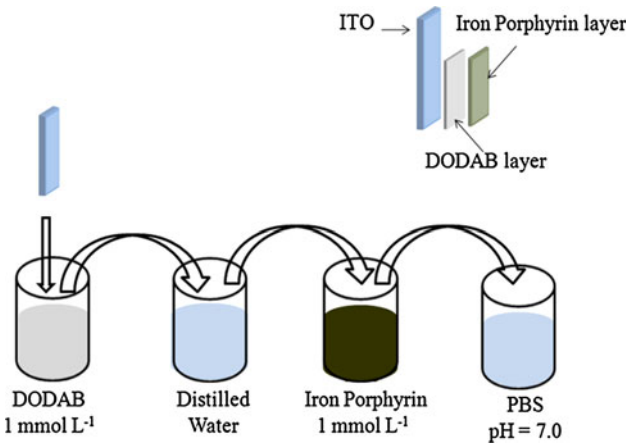

Fig. 2 Schematic representation of the formation of a bilayer film of ITO-(DODAB/Porphyrin iron) by the LBL technique

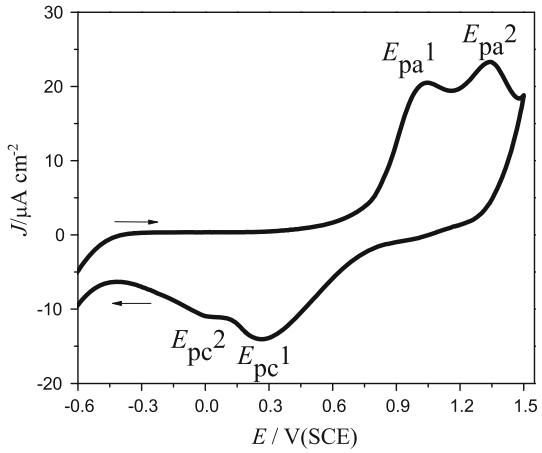

Fig. 3 Cyclic voltamogram for 5-bilayer LbL films of ITO-DODAB/$Fe^{3+}TDCSO_3{}^{-}Na^{+}PP$. Scan rate: 100 mV s^{-1}. Phosphate buffer: 0.1 mol L^{-1}

of different redox processes for porphyrins in non-aqueous [56–60] and aqueous [61–63] homogeneous media. For instance, Kaaret et al. [58] observed the dependence of the oxidation potential of the Fe^{3+} porphyrin redox couple as a function of the electrolyte pH. Considering that at least one metal-centered redox process is present in the system described here, the one electron oxidation of porphyrin Fe^{3+} exhibiting water as the axial ligand is expected to generate oxoferryl species (Fe^{4+}=O) rather than Fe^{4+} form. Liu et al. [41] observed the formation of oxoferryl species at 0.75–1.35 V for $TSMPFe^{+3}$ (Fe^{3+} *meso*-tetrakis(3-sulfonatomesityl)porphyrin) at different pH values. In the pH range from 6.0 to 10.0, the authors observed two oxidation processes and proposed the following reaction (Eq. 1):

$$(TSMPyP)Fe^{+3}(OH) \rightleftarrows (TMPyP)Fe^{+4} = O + e^{-} + H^{+} \quad (1)$$

Similarly Rana and Tamagake described the generation of oxo-ferryl porphyrins by the electrochemical oxidation of

(HO)FeIIITMPyP [43]. In this regard, the electrochemical formation of the oxoferryl species via electrochemical oxidation of Fe^{3+} porphyrins has been corroborated by spectroelectrochemisty [41, 42] focusing spectral analysis in the fingerprint absorbing wavelength regions for the porphyrins: the Soret (400 nm region) and Q bands (500–600 nm region).

Thus, supported by several previous studies, the 1.0 and 1.3 V potentials presented in Fig. 3 may be assigned to the oxidation of the center metal and porphyrin ring, respectively.

The implications for the electron tunneling observed in the supramolecular LbL arrangement could be related to changes in the porphyrin structure. It is well-known that the spin density and molecule polarization influence the charge transfer along the perpendicular oriented direction of the metalloporphyrin layers on a solid substrate. Therefore, total energy ab initio calculation based on spin-polarized density functional theory (DFT) was performed to better understand the conditions responsible for the electroactivity of the metalloporphyrin layers intercalated by an insulating material.

Total energy ab initio DFT calculations were performed for the surfactant bilayer, for the metalloporphyrin, and for the supramolecular arrangement of the metalloporphyrin associated to the cationic interface. As a strategy to facilitate the calculation, the structure of a parent surfactant with the shorter hydrocarbon chain ditetradecyldimethylammonium bromide (DTDAB) replacing DODAB was used. The DTDAB molecule calculated structure, shown in the Fig. 4, presents the hydrocarbon chains arranged in a scissor conformation. The distances between the carbon atoms in the adjacent layers are consistent with the scissor conformation. Consistently the carbon–carbon distances progressively increases from 4.29 Å for pair 1 to the maximal distance of 5.97 Å at pair 8 and then progressively decreases to the minimal distance of 2.54 Å for pair 14. Arranged as a lipid bilayer, the DTDAB molecules are in neutral configuration, presenting no polarization.

Figure 5 shows the computed local magnetization density, $m(\vec{r}) = \rho_{\mathrm{up}}(\vec{r}) - \rho_{\mathrm{down}}(\vec{r})$, of the isolated, DTDAB-free, metallophorphyrin. The iron *d* orbital in the central position of the porphyrin molecule exhibits the iso-surface in an almost spherical shape (negative value) that polarizes the N-*p* orbitals in a positive way.

Figure 6 shows the magnetization density iso-surfaces, $m(\vec{r}) = \rho_{\mathrm{up}}(\vec{r}) - \rho_{\mathrm{down}}(\vec{r})$, calculated for the metallophorphyrin and DTDAB molecules in the associated form. The association to DTDAB bilayer led the porphyrin to assume a less distorted configuration consistent with the bond distances from the KS-DFT LDA calculations.

The result obtained for the metalloporphyrin-free system is different from the spin densities for the complex and now we can see some polarization around the atoms of the DTDAB head groups. As a result, the spin moment of the whole metalloporphyrin molecule decreases from 2.00 to 1.73 μB for the lipid-interacting molecule. It is noticeable that the net difference in the spin moment of the metalloporphyrin promoted by the association with the bilayer was higher than that described for in situ-sublimated Fe porphyrin molecules on ferromagnetic Ni and Co films on Cu(100) [64]. In this condition, the authors found a slight increase in the spin moment of the whole porphyrin molecule from 2.00 μB for the free molecule to 2.17 μB for the deposited molecule. This difference was related to the Co surface and the authors had studied the interactions between magnetic systems. Our focus here is to understand the polarization in the DTDAD induced by the porphyrin molecule.

The metalloporphyrin-induced DTDAB polarization obtained by theoretical calculation is consistent with electron tunneling observed for the LbL construct.

The experimental approaches used to monitor the changes in the porphyrin structure induced by the association with a cationic ammonium quaternary surfactant were electron paramagnetic resonance and magnetic circular dichroism. Both techniques suggested the presence of two porphyrin conformations induced by the association with DODAB bilayers with a signal contribution from a more rhombic species. An EPR analysis of the porphyrin in the homogeneous medium (Fig. 7a, line a = experimental spectrum and line b = simulation with g parameters = 5.99, 5.80, 2.00) and of the porphyrin associated to DODAB revealed, in the latter, the presence of two high-spin Fe(III) porphyrin populations associated with DODAB vesicles (Fig. 7b, line a = experimental spectrum, and line b = simulation with two components showed as lines c and d). The most abundant component (75%, line c) presents g values (6.10, 5.96, 2.00) indicative of porphyrin molecules with lower rhombicity (g_x–g_y) relative to the homogeneous media. The less abundant component (25%, line d), with g values 7.02, 5.15, and 2.00, is consistent with a more rhombic porphyrin structure.

An increase in the rhombicity in a fraction of the porphyrin content was also corroborated by MCD spectroscopy (Fig. 8). Both free and surfactant-bound high-spin forms of $Fe^{3+}TDCSO_3^-Na^+PP$ exhibit asymmetrical "S"-shaped bands in the Soret region. DODAB liposomes promoted significant $\Delta\varepsilon$ decrease in the negative MCD band in the Soret region, slight decrease in the positive band $\Delta\varepsilon$ at the same region and shifted the zero crossing to lower energy. Due to the presence of a partially filled set of *d*-orbitals, the electronic absorption of $Fe^{3+}TDCSO_3^-Na^+PP$ at the Soret region results from the contribution of

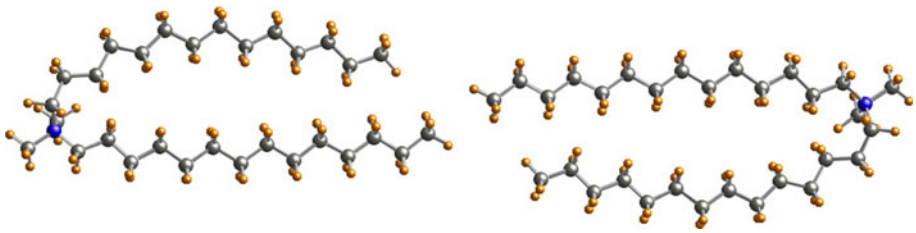

Fig. 4 Ball and stick representation of DTDAB molecules in a bilayer arrangement with the *orange* small spheres representing the hydrogens, the *gray* ones for the carbons, and the *blue* show the nitrogen atom. Magnetization density calculated for the DTDAB molecules arranged as bilayer indicating absence of magnetization in the absence of $Fe^{3+}TDCSO_3^-Na^+PP$

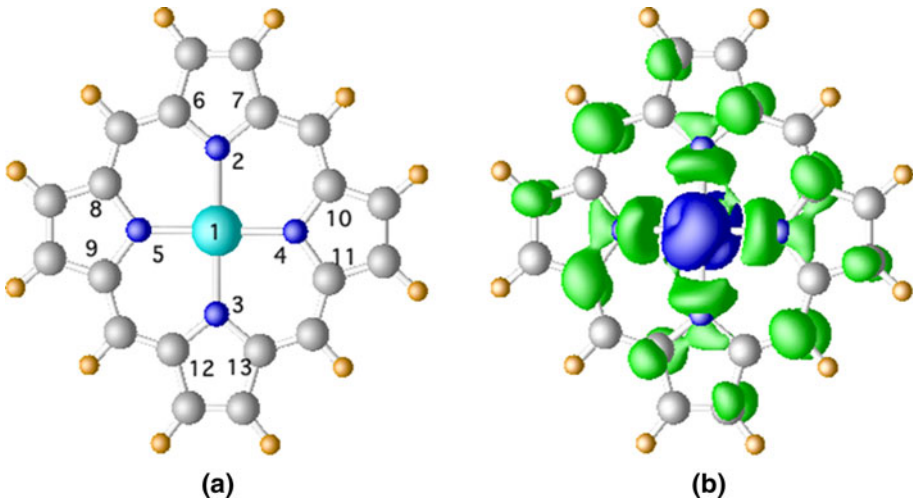

Fig. 5 **a** Schematic illustration of $Fe^{3+}TDCSO_3^-Na^+PP$ chloride molecule in a ball and stick format; **b** local magnetization density, $m(\vec{r}) = \rho_{up}(\vec{r}) - \rho_{down}(\vec{r})$, calculated by ab initio calculations for the free $Fe^{3+}TDCSO_3^-Na^+PP$ molecule. The magnetization iso-surfaces are represented in *blue* (negative) and in *green* (positive). The atom positions are as follows: C, *gray*; H, *orange*; N; *blue*, Fe, *cyan*

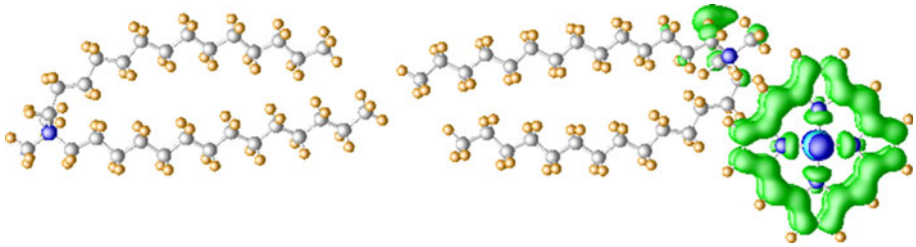

Fig. 6 Local magnetization, $m(\vec{r}) = \rho_{up}(\vec{r}) - \rho_{down}(\vec{r})$, for the system phorphyrin DTDAB-lime molecules. The magnetization density iso-surfaces values are 0.003 (*green*) and −0.05 (*blue*) e/°A^3 and are represented in *blue* (negative) and in *green* (positive)

ligand to metal and metal to ligand charge transfer transitions (LMCT, MLCT) in addition to the $\pi \rightarrow \pi^*$ transitions resulting in the complex UV–visible signal [65]. As a non-chiral molecule with molecular orbital degeneracy, $Fe^{3+}TDCSO_3^-Na^+PP$ does not exhibit circular dichroism (CD) signal. The presence of a magnetic field results in the magnetic circular dichroism signal as resulting from orbital splitting (Faraday A term contribution) and mixing (Faraday B term contribution) [38, 66–68].

In homogeneous media, $Fe^{3+}TDCSO_3^-Na^+PP$ exhibits a MCD spectrum (Fig. 8a) with the zero crossing that matched closely with the electronic absorption maximum (Fig. 8b). However, in DODAB liposomes, $Fe^{3+}TDCSO_3^-Na^+PP$ exhibited a decrease in the negative band due to larger symmetry-breaking distortions of the porphyrin in the heterogeneous medium. This feature arises from the contributions of the temperature-independent term [19, 58, 69]. The S shape and zero crossing of the MCD spectra matched with the electronic absorption maximal most probably results from the magnetic field-induced split of degenerated iron *d*-orbitals (Faraday A term). In addition, the charge transfer Soret band component is overlapped by the contribution of

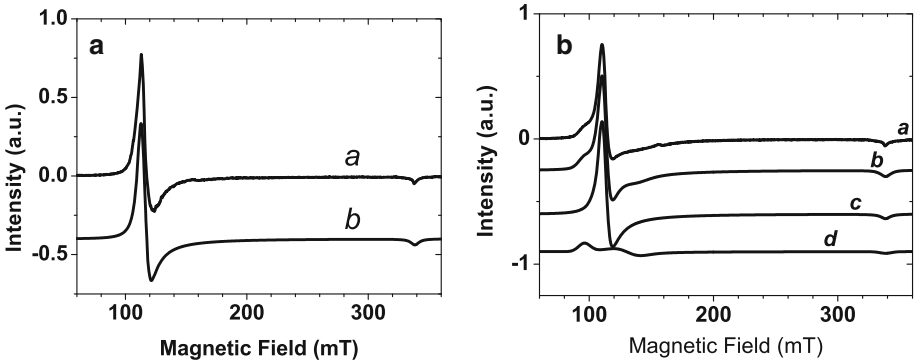

Fig. 7 **a** Experimental EPR spectra of 100 μM $Fe^{3+}TDCSO_3^{-}Na^{+}PP$ in 200 mM HEPES buffer, pH 7.5 (line *a*), and the corresponding simulated spectrum (line *b*). **b** Experimental EPR spectrum of Fe^{3+} $TDCSO_3^{-}Na^{+}PP$ associated with DODAB liposomes (line *a*), corresponding simulated EPR spectrum (line *b*), and EPR spectrum of the components (lines *c* and *d*)

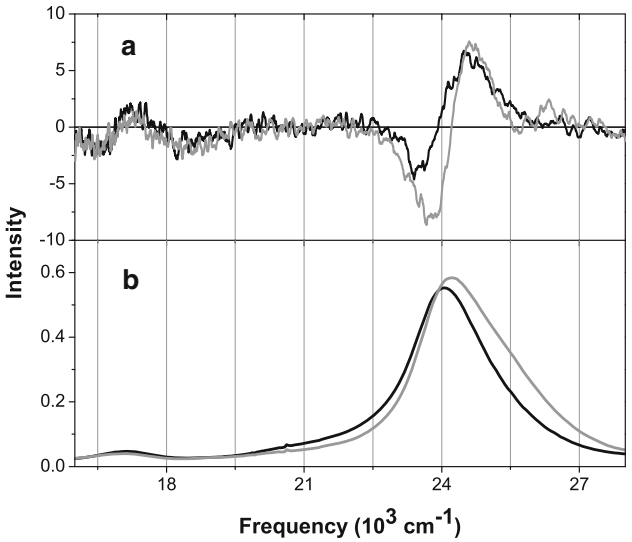

Fig. 8 MCD (**a**) and Electronic absorption (**b**) spectra of 150 μM $Fe^{3+}TDCSO_3^{-}Na^{+}PP$ in 200 mM HEPES buffer, pH 7.5 (*gray lines*), and 150 μM $Fe^{3+}TDCSO_3^{-}Na^{+}PP$ in DODAB liposomes (*black lines*)

π–π^* transitions. For the latter transition, MCD bands result from preferential absorption of left and right circularly polarized light (lcp and rcp, respectively) that were made feasible by the mixing of an intermediate state (|K>) with an excited state (|J>) by the applied field.

Therefore, the decrease in the negative MCD Soret band signal suggests an increased contribution from an overlapping absorption shape positive band (Faraday B term) promoted by a significant symmetry break distortion of the porphyrin structure as predicted by the KS-DFT LDA calculations. EPR data revealed changes in the $Fe^{3+}TDCSO_3^{-}Na^{+}PP$ structure in the presence of DODAB resulting in a gain of symmetry by most of the metalloporphyrin population and loss of symmetry by a less abundant population. Considering that spectroscopic data were obtained for the suspension of DODAB vesicles associated to the metalloporphyrin, it is possible the existence of a population of porphyrins deposited on the DODAB vesicle surface and another population of porphyrins bridging two DODAB vesicles via electrostatic interactions with the surfactant cationic head groups which is probably in a more symmetric conformation relative to the free porphyrin. The results obtained from the KS-DFT LDA calculations best represent the former metalloporphyrin population that is expected to be predominant population in the LbL organization of DODAB bilayers and porphyrin.

4 Conclusions

In this work, we have shown that magnetic coupling between $Fe^{3+}TDCSO_3^{-}Na^{+}PP$ and the DTDAB molecule is a probable contributing factor to the electron hopping responsible for the electroactivity of LbL constructed by alternating layers of the metalloporphyrin and DODAB bilayer. This finding is important in the fields of molecular, supramolecular, and organic electronics. More experimental work needs to be performed to fully characterize the structure and other properties of this system, including low-temperature MCD experiments. In addition, high level WFT methods, like CASPT2 [35] and MR-CC [36, 37, 39, 40], and the recently developed semi-empirical KS LC-DFT, KS LC_{gau}-DFT, KS LC-DFT+LRD, and KS LC_{gau}-DFT+LRD [34] or ab inito KS-DFT methods using multi-reference (MR) optimized effective potentials (OEPs) will allow one to get quantitative numbers. The numbers we have reported here at LDA KS-DFT level using a single reference (SR) configuration can only be expected to give qualitative accuracy.

Acknowledgments We are grateful to FAPESP, CNPq, and CAPES. KCUM is research fellow supported by a FAPESP fellowship. We thank also to Karl J. Jalkanen, FAPESP-supported visitor professor of Universidade do Vale do Paraíba (UNIVAP), Brazil for

the invitation to contribute our work to the Imamura Festschrift Issue of TCA and by the critical reading and comments contributing to improve the manuscript. We thank UFABC and CENAPAD-Campinas/SP (Centro Nacional de Processamento de Alto Desempenho) for the computational facilities.

References

1. Nantes IL, Mugnol KCU (2008) Incorporation of respiratory cytochromes in liposomes: an efficient strategy to study the respiratory Chain. J Liposome Res 18:175–194
2. Dmitri B, Ponomarev GV, Trettnak W, O'Leary P (1995) Phosphorescent complexes of porphyrin ketones: optical properties and application to oxygen sensing. Anal Chem 67:4112–4117
3. Clyde-Watson Z, Vidal-Ferran A, Twyman LJ, Walter CJ, McCallien DWJ, Fanni S, Bampos N, Wylie SR, Sanders JKM (1998) Reversing the stereochemistry of a Diels–Alder reaction: use of metalloporphyrin oligomers to control transition state stability. New J Chem 22:493–502
4. Qiana D-J, Wenka S-O, Nakamuraa C, Wakayamaa T, Zorinb N, Miyakea J (2002) Photoinduced hydrogen evolution by use of porphyrin, EDTA, viologens and hydrogenase in solutions and Langmuir–Blodgett films. Int J Hydrogen Energy 27:1481–1487
5. Imahori H (2004) Giant multiporphyrin arrays as artificial light-harvesting antennas. J Phys Chem B 108:6130–6143
6. Lin VS-Y, DiMagno SG, Therien MJ (1994) Highly conjugated, acetylenyl bridged porphyrins: new models for light-harvesting antenna systems. Science 264:1105–1111
7. Gust G, Moore TA (1989) Mimicking photosynthesis. Science 244:35–41
8. Hu X, Ritz T, Damjanovic A, Autenrieth F, Schulten KQ (2002) Photosynthetic apparatus of purple bacteria. Quart Rev Biophys 35:1–62
9. Berg JM, Tymoczko JL, Stryer L (2006) Biochemistry. W. H. Freeman and Company, New York
10. Gray HB (2003) Biological inorganic chemistry at the beginning of the 21st century. Proc Natl Acad Sci USA 100:3563–3568
11. Shi Y (2001) A structural view of mitochondria-mediated apoptosis. Nat Struct Biol 8:394
12. Kuehl CJ, Tabellion FM, Arif AM, Stang PJ (2001) Single- and double-stranded chains assembled viaconcomitant metal coordination and hydrogen bonding. Organometallics 20:1956–1959
13. Pradilla-Sorzano J, Fackler JP Jr (1973) Base adducts of beta-ketoenolates. V. Crystal and molecular structure of cis-bis(1, 1, 1, 6, 6, 6-hexafluoro-2, 4-pentanedionato)bis(pyridine)zinc(II) and copper(II). Inorg Chem 12:1174–1182
14. Schmitz M, Leininger S, Fan J, Arif AM, Stang PJ (1999) Preparation and solid-state properties of self-assembled dinuclear platinum(II) and palladium(II) rhomboids from carbon and silicon tectons. Organometallics 18:4817–4824
15. Bernien M, Miguel J, Weis C, Ali ME, Kurde J, Krumme B, Panchmatia PM, Sanyal B, Piantek M, Srivastava P, Baberschke K, Oppeneer PM, Eriksson O, Kuch W, Wende H (2009) Tailoring the nature of magnetic coupling of fe-porphyrin molecules to ferromagnetic substrates. Phys Rev Lett 102:047202
16. Grill L, Dyer M, Lafferentz L, Persson M, Peters MV, Stefan Hecht S (2007) Nano-architectures by covalent assembly of molecular building blocks. Nat Nanotech 2:687–691
17. Scheybal A, Ramsvik T, Bertschinger R, Putero M, Nolting F, Jung TA (2005) Induced magnetic ordering in a molecular monolayer. Chem Phys Lett 411:214–220
18. Wende H, Bernien M, Luo J, Sorg C, Ponpandian N, Kurde J, Miguel J, Piantek M, Xu X, Eckhold P, Kuch W, Baberschke K, Panchmatia PM, Sanyal B, Oppeneer PM, Eriksson O (2007) Substrate-induced magnetic ordering and switching of iron porphyrin molecules. Nat Mater 6:516–520
19. Frandsen C, Bahl CRH, Lebech B, Lefmann K, Kuhn LT, Keller L, Andersen NH, Zimmermann M, Johnson E, Klausen SN, Mørup S (2005) Oriented attachment and exchange coupling of α-Fe2O3 nanoparticles. Phys Rev B 72:214406
20. Bernien M, Xu X, Miguel J, Piantek M, Eckhold P, Luo J, Kurde J, Kuch W, Baberschke K, Wende H, Srivastava P (2007) Fe-porphyrin monolayers on ferromagnetic substrates: electronic structure and magnetic coupling strength. Phys Rev B 76:214406
21. Prieto T, Mugnol KCU, Araujo JC, Souza FL, Soares VA, Cilento G, Nantes IL (2007) Peroxidase model systems in heterogeneous media. In: Nantes IL, Brochsztain S (eds) Catalysis and photochemistry in heterogeneous media, 1st edn. Research Signpost, India, Kerala, p 1. ISBN:978-81-308-0168-1
22. Swiegers GF, Malefeste TJ (2000) New self-assembled structural motifs in coordination chemistry. Chem Rev 100:3483–3537
23. Lehn JM (1995) Supramolecular chemistry concepts and perspectives. VCH, Weinheim, pp 139–160
24. Robson R (1996) In: Atwood JL, Davies JED, MacNicol DD, Vögtle F, Toda F, Bishop R (eds) Comprehensive supramolecular chemistry, vol 6. Pergamon, Oxford, p 733
25. Lenninger S, Olenyuk B, Stang P (2000) Self-assembly of discrete cyclic nanostructures mediated by transition metals. Chem Rev 100:853–907
26. Uller E, Demleitner B, Bernt I, Saalfrank RW (2000) Synergistic effect of serendipity and rational design in supramolecular chemistry. In: Fujita M (ed) Structure and bonding, vol 96. Springer, Berlin, p 149
27. Oshovsky GV, Reinhoudt DN, Verboom W (2007) Supramolecular chemistry in water. Angew Chem Int Ed 46(14):2366–2393
28. Piguet C, Bernardinelli G, Hopfgartner G (1997) Helicates as versatile supramolecular complexes. Chem Rev 97:2005–2062
29. Bartlett RJ, Lotrich VF, Schweigert IV (2005) Ab initio density functional theory: the best of both worlds? J Chem Phys 123:062205
30. Bartlett RJ, Schweigert IV, Lotrich VF (2006) Ab initio DFT: getting the right answer for the right reason. J Mol Struct: Theochem 771:1–8
31. Chaia J-D, Head-Gordon M (2008) Systematic optimization of long-range corrected hybrid density functional. J Chem Phys 128:084106
32. Fan J, Autschbach J, Ziegler T (2010) Electronic structure and circular dichroism of tris(bipyridyl) metal complexes within density functional theory. Inorg Chem 49:1355–1362
33. Xue ZL, Mack J, Lu H, Zhang L, You XZ, Kuzuhara D, Stillman M, Yamada H, Yamauchi S, Kobayashi N, Shen Z (2011) The synthesis and properties of free-base [14] triphyrin (2.1.1) Compounds and the formation of subporphyrinoid metal complexes. Chem Eur J 17:4396–4407
34. Song J-W, Tsuneda T, Sato T, Hirao K (2011) An examination of density functional theories on isomerization energy calculations of organic molecules. Theor Chem Acc. doi:10.1007/s00214-011-0997-6
35. Boos BO (2008) Multiconfigurational quantum chemistry for ground and excited states. In: Shukla MK, Leszczynski J (eds) Radiation induced molecular phenomena in nucleic acids. Springer, Heidelberg, pp 125–156
36. Tobita M, Perera SA, Musial M, Bartlett RJ, Nooijen M, Lee JS (2003) Critical comparison of single-reference and multireference coupled-cluster methods: Geometry, harmonic frequencies, and excitation energies of N_2O_2. J Phys Chem 119:10713–10723
37. Mahapatra US, Chattopadhyay S (2011) Application of the uncoupled state-specific multireference coupled cluster method to a weakly bonded system: exploring the ground state Be_2. J Phys B: At Mol Opt Phys 44:105102–105114

38. De Luca G, Romeo A, Scolaro LM, Ricciardi G, Rosa A (2009) Sitting-atop metallo-porphyrin complexes: experimental and theoretical investigations on such elusive species. Inorg Chem 48:8493–8507
39. Saito T, Nishihara S, Yamanaka S, Kitagawa Y, Kawakami T, Yamada S, Isobe H, Okumura M, Yamaguchi K (2011) Symmetry and broken symmetry in molecular orbital description of unstable molecules IV: comparison between single- and multi-reference computational results for antiaromtic molecules. Theor Chem Acc. doi:10.1007/s00214-011-0941-9
40. Saito T, Nishihara S, Yamanaka S, Kitagawa Y, Kawakami T, Yamada S, Isobe H, Okumura M, Yamaguchi K (2011) Singlet–triplet energy gap for trimethylenemethane, oxyallyl diradical, and related species: single- and multireference computational results. Theor Chem Acc. doi:10.1007/s00214-011-0914-z
41. Paterno LG, Mattoso LHC, Oliveira ON Jr (2001) Filmes poliméricos ultrafinos produzidos pela técnica de automontagem: preparação, propriedades e aplicações. Quim Nova 24:228–235
42. Crespilho FN, Silva WC, Zucolotto V Supramolecular assemblies of metallophthalocyanines: Physicohemcial properties and aplications. In: Nantes IL, Brochsztain S (eds) Peroxidase model system in heterogeneous media in catalysis and photochemistry in heterogeneous media, 1st edn. Research Signpost, India, Kerala
43. Vidotti M, Silva MR, Salvador RP, Torresi SIC, Dall'Antonia LH (2008) Electrocatalytic oxidation of urea by nanostructured nickel/cobalt hydroxide electrodes. Electrochim Acta 53:4030
44. Watanabe S, Kimura H, Sato T, Shibata H, Sakamoto F, Azumi R, Sakai H, Abe M, Matsumoto M (2008) Micro- and nanopatterned copper structures using directed self-assembly on templates fabricated from phase-separated mixed Langmuir—Blodgett films. Langmuir 24:8735
45. Mandal P, Srinivasa RS, Talwar SS, Major SS (2008) CdS/ZnS core-shell nanoparticles in arachidic acid LB films. Appl Surf Sci 254:5028
46. Decher G (1997) Fuzzy nanoassemblies: toward layered polymeric multicomposites. Science 277:1232–1237
47. Decher G, Eckle M, Struth B, Schmitt J (1998) Layer-by-layer assembled multicomposite films. Curr Opin Coll Interface Sci 3:32–39
48. Kresse G, Joubert D (1999) From ultrasoft pseudopotentials to the projector augmented-wave method. Phys Rev B 59:1758–1775
49. Blöchl PE (1994) Projector augmented-wave method. Phys Rev B 50:17953–17979
50. Arantes JT, Lima MP, Fazzio A, Xiang HJ, Wei SH, Dalpian GM (2009) Effects of side-chain and electron exchange correlation on the band structure of perylene diimide liquid crystals: a density functional study. J Phys Chem B 113:5376–5380
51. Crespilho FN, Zucolotto V, Oliveira ON Jr, Nart FC (2006) Electrochemistry of Layer-by-Layer films: a review. Int J Electrochem Sci 1:194–214
52. Siqueira JR Jr, Gasparotto LHS, Crespilho FN, Carvalho AJF, Zucolotto V, Oliveira ON Jr (2006) Physicochemical properties and sensing ability of metallophthalocyanines/chitosan nanocomposites. J Phys Chem B 110:22690–22694
53. Crespilho FN, Zucolotto V, Brett CMA, Oliveira ON Jr, Nart FC (2006) Enhanced charge transport and incorporation of redox mediators in layer-by-Layer films containing PAMAM-encapsulated gold nanoparticles. J Phys Chem B 110:17478–17483
54. Crespilho FN, Huguenin F, Zucolotto V, Olivi P, Nart FC, Oliveira ON Jr (2006) Dendrimers as nanoreactors to produce platinum nanoparticles embedded in layer-by-layer films for methanol-tolerant cathodes. Electrochem Commun 8:348–352
55. Laurent D, Schlenoff JB (1997) Multilayer assemblies of redox polyelectrolytes. Langmuir 13:1552–1557
56. Barley MH, Takeuchi KJ, Meyer TJ (1986) Electrocatalytic reduction of nitrite to ammonia based on a water-soluble iron porphyrin. J Am Chem Soc 108:5876–5885
57. Chen S-M, Chiu S-W (2000) The electrocatalytic transformation of HS^-, $S_2O_3^{2-}$, $S_4O_6^{2-}$ and SO_3^{2-} to SO_4^{2-} and SO_3^{2-} to SO_4^{2-} by water-soluble iron porphyrins. Electrochim Acta 45: 4399–4408
58. Kaaret TW, Zhang G-H, Bruice TC (1991) Electrochemistry and the dependence of potentials on pH of iron and manganese tetraphenylporphyrins in aqueous solution. J Am Chem Soc 113:4652–4656
59. Kadish KM, Caemelbecke EV, D'Souza F, Gueletii E, Fukuzumi S, Miyamoto K, Suenobu T, Tabard A, Guilard R (1998) Kinetic and thermodynamic studies of iron(III) and iron(IV) σ–bonded porphyrins. Formation and reactivity of $[(OEP)Fe(R)]^{n+}$, where OEP Is the dianion of octaethylporphyrin ($n = 0$, 1, 2, 3) and R = C_6H_5, 3, 4, 5–$C_6F_3H_2$, 2, 4, 6–$C_6F_3H_2$, C_6F_4H, or C_6F_5. Inorg Chem 37:1759–1766
60. Kadish KM, Caemelbecke EV, D'Souza F, Medforth CJ, Smith KM, Tabard A, Guilard R (1993) Generation of a stable σ-bonded iron(1 V) porphyrin. Formation and reactivity of $[(OETPP)Fe^{IV}(C_6H_5)]^{n+}$ (n = 1–3; OETPP = dianion of 2, 3, 7, 8, 12, 13, 17, 18-octaethyl-5, 10, 15, 20-tetraphenylporphyrin. Organometallics 12:2411–2413
61. Liu M-H, Su YO (1998) Selective electrocatalysis of alkene oxidations in aqueous media. J Electroanal Chem 452:113–125
62. Lei J, Ju H, Ikeda O (2004) Catalytic oxidation of nitric oxide and nitrite mediated by water-soluble high-valent iron porphyrins at an ITO electrode. J Electroanal Chem 567:331–338
63. Rana MS, Tamagak K (2005) Formation of ferryl porphyrin by electrochemical reduction of iron porphyrin in aqueous solution. J Electroanal Chem 581:145–152
64. Chylarecka D, Kim TK, Tarafder K, Mller K, Gdel K, Czekaj I, Wckerlin C, Cinchetti M, Ali ME, Piamonteze C, Schmitt F, Wüstenberg JP, Ziegler C, Nolting F, Aeschlimann M, Oppeneer PM, Ballav N, Jung TA (2011) Indirect magnetic coupling of manganese porphyrin to a ferromagnetic cobalt substrate. J Phys Chem C 115:1295–1301
65. Nantes IL, Crespilho FN, Mugnol KCU, Araújo-Chaves JC, Luz RAS, Otaciro Rangel Nascimento OR, Pinto SMS (2010) Magnetic circular dichroism applied in the study of symmetry and functional properties of porphyrinoids. In: David S. Rodger (eds) Circular dichroism: theory and spectroscopy. Nova Science Publishers, Inc., USA. ISBN: 978-1-61122-522-8
66. Kobayashi N, Nakai K (2007) Applications of magnetic circular dichroism spectroscopy to porphyrins and phthalocyanines. Chem Commun 4077–4092
67. Macka J, Stillman MJ, Kobayashi N (2007) Application of MCD spectroscopy to porphyrinoids. Coord Chem Rev 251:429–453
68. Suchkova SA, Soldatov A, Dziedzik-Kocurek K, Stillman MJ (2009) The role of spin state on the local atomic and electronic structures of some metalloporphyrin complex. J Phys: Conf Ser 190:012211
69. Solheim H, Ruud K, Coriani S, Norman P (2008) The A and B terms of magnetic circular dichroism revisited. J Phys Chem A 112:9615–9618